AD 688861

TECHNICAL REPORT

WVT-6905

TWO-DIMENSIONAL PHOTOELASTIC INVESTIGATION OF STRESSES IN RIFLING PROJECTIONS

BY

G. PETER O'HARA

D D C

JUN 23 1969

APRIL 1969

BENET R&E LABORATORIES

WATERVLIET ARSENAL

WATERVLIET—NEW YORK

AMCMS No. 5025.11.29900

DA Project No. 1C024401A349

34

TWO-DIMENSIONAL PHOTOELASTIC INVESTIGATION

OF STRESSES IN RIFLING PROJECTIONS

ABSTRACT

The problem of stress concentrations in rifling projections, caused by two independent simultaneous loads, is investigated experimentally using the two-dimensional photoelastic technique. A tensile field stress and a side bearing stress were applied to a series of photoelastic models and stress concentration determined for a large range of widths and fillet radii.

The stress concentration factor is presented in terms of non-dimensional width, non-dimensional fillet radius and a factor relating the two loads. This presentation clearly shows the decrease in stress concentration with increasing fillet radius and width, which allows the design engineer to evaluate the trade-offs of changing fillet radius or width in establishing the shape of rifling projections.

Cross-Reference
Data

Photoelasticity

Photoelastic
Investigation

Rifling
Projections

Stress Concen-
trations

1

TABLE OF CONTENTS

FIGURES

2

TABLES

3

LIST OF SYMBOLS

h   =   Height of projection

r   =   Fillet radius

w   =   Width of the top of the projection

$\bar{R}$ =   Nondimensional fillet radius $(\frac{r}{h})$

$\bar{W}$ =   Nondimensional width $(\frac{W}{h})$

T   =   Average tensile stress

B   =   Average bearing stress (based on full height)

$\bar{L}$ =   Loading (factor) $\dfrac{\sigma B}{\sigma T}$ $\dfrac{\text{average bearing stress}}{\text{average tensile stress}}$

N_M =   Maximum fringe order in model

N_N =   Average nominal fringe order

K_T =   Stress concentration based on sheet stress

4

INTRODUCTION

It is a very difficult and complicated task to describe, theoretically, the total state of stress in a gun tube subjected to an internal propellant gas pressure. Some of the significant factors which should be taken into consideration in the design of a gun tube are:

1. Stress from gas pressure as calculated from the Lamé Equation.

2. Thermal stress.

3. Transient effects in the vicinity of the projectile.

4. Bearing stress caused by the torque of the projectile on the rifling.

5. Residual stress.

6. Inertial and vibration stesses.

Because of the many variables, the solution of stresses in gun tubes must first be broken down into smaller parametric studies of workable size and solved for a wide range of variables, before the overall picture can be properly evaluated. This paper gives results for one of these small parametric studies using the two-dimensional photoelastic method.

This study deals with two loads on the rifling projections and attempts to apply these loads to a large range of geometries. The first load is tangential stress, which has been looked at in great detail by Radkowski, Bluhm and Bowie[1]. The second load of importance in rifling is the side bearing load caused by the acceleration of the projectile[2,3]. A more critical look at the possible effects of the shape of the rifling seemed necessary in view of the fatigue problem caused by the requirement for increased performance.
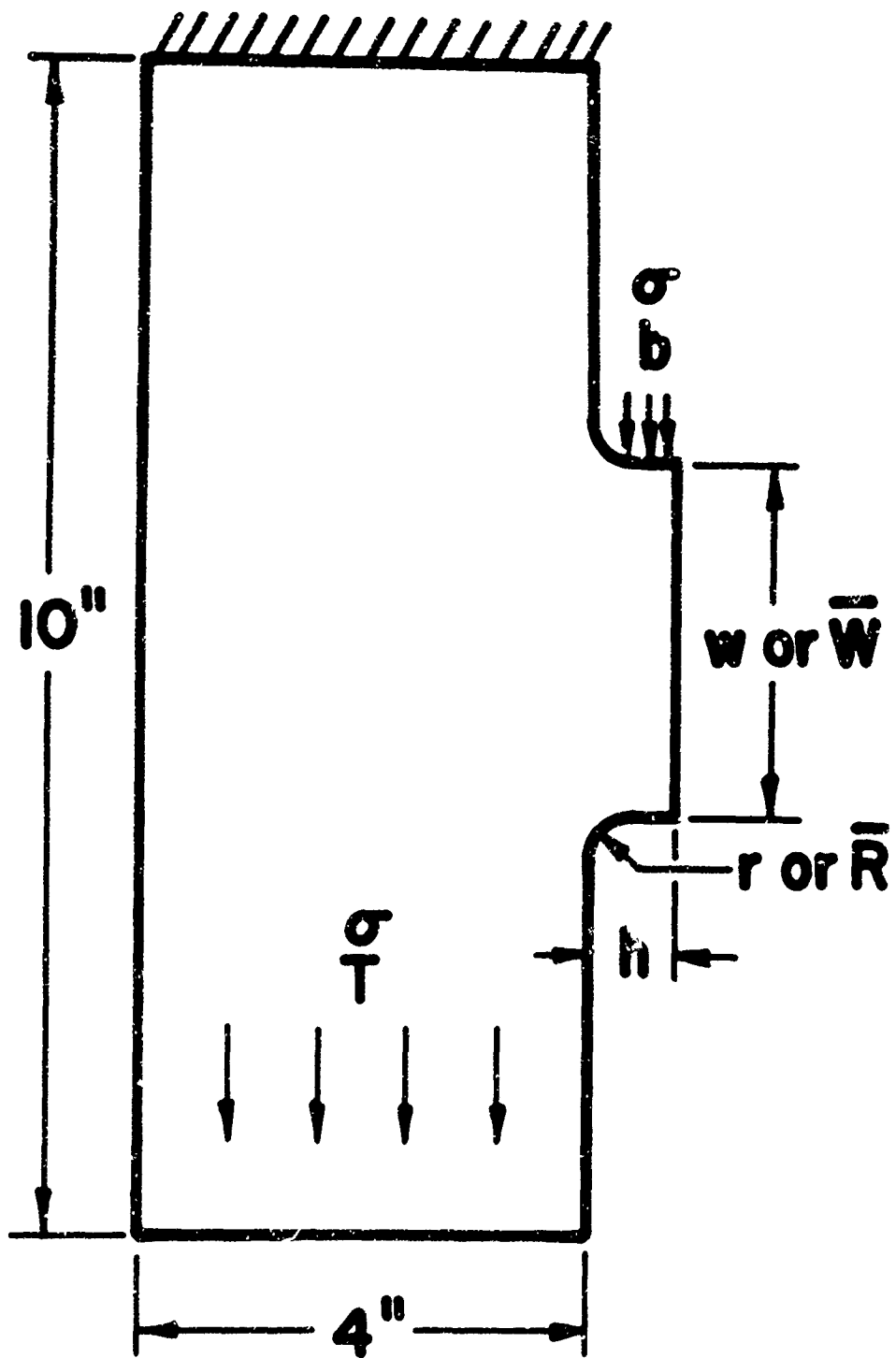
5

Figure 1. Drawing showing geometry and applied loads.

Rifling was characterized as a square projection of a stressed surface with some fillet radius, r, a height, h, and width, w. (Figure 1). This was put in non-dimensional form by dividing by h, and the two non-dimensional factors are width, $\overline{W}$, and radius, $\overline{R}$. The loads were non-dimensionalized by dividing the bearing stress σ_B by the tensile field stress σ_T to give the non-dimensional loading factor, $\overline{L}$. It was decided to test five models which would cover a range of radius $(\overline{R})$ from 0.1 to 1.0 and $\overline{W}$ from 5.0 to 0.5 and a range of $\overline{L}$ of 0 to 2.0. The two-dimensional photoelastic method was selected as the best way to survey fillet stress as determined by stress concentration factor (K_T). This factor is the maximum tensile fillet stress (σ_{max}) divided by the tensile field stress (σ_T). A method of applying both loads simultaneously was determined to be experimentally sound.

7

MODELS

The models were fabricated from Photolastic Inc., PSM-IF sheet. This is available in 10" x 10" x .250" size. This established the 10" x 4" model size and the .75" projection height which allowed two models to be cut from each sheet of material. Five models were fabricated at the $\bar{W} = 5$ level from precision steel templates. Each of the models had an appropriate radius to produce $\bar{R}$ equal 1.0, 0.9, 0.5, 0.3 and 0.1. These models were then successively modified for the other $\bar{W}$ levels of 2, 1 and 1/2. It was found necessary to oven-cure the models after each machining operation to eliminate all residual fringes and the following temperature cycle was used:

1. Rise at 15° per hour to 250°F.

2. Hold at 250°F for 4 hours.

3. Decay at 5°F per hour to room temperature.

The models were then stored in a dessicator until they could be tested which was often several weeks after annealing. It was later found that this storage was necessary to obtain good humidity balance so that no zero load fringe order would be present.

8

TESTING PROCEDURE

The model was gripped by bolting the ends between 1/4" steel plates (Figure 2); then the top of the model was fixed to the top of the loading frame using two pins (Figure 3). The tensile load was applied to the bottom by a pinned link using the top loading bar to produce the tensile field stress. It was necessary to adjust bolt tensions and the model position to produce the most nearly uniform fringe order in the body of the model. The bearing stress was applied with a set of .60" form fitted steel loading blocks, with a thin rubber pad between the blocks and the model. The loading blocks were attached to the bottom loading bar using light stranded wire. For the radii greater than $\overline{R} = 0.5$, it was necessary to use a side reaction support to keep the loading block in the proper position on the model. The bearing stress blocks and wires may be seen in the fringe photographs. This method allowed the bearing load to be applied without appreciably blocking the view of the model.

The loads used were limited by two considerations: (1) The loading weights available for the test, and (2) readability of the fringe orders photographed. Therefore, tensile loads of 200, 100 or 50 pounds were used and bearing loads of 75, 50, 25 or 18-3/4 pounds were used in various combinations to produce the proper loading factors of 0, 0.66, 1.33 and 2.00.

A basic tension load of 200 pounds was applied to the model and the nominal fringe order was measured at this load by averaging the order determined by Tardy compensation at three locations. The
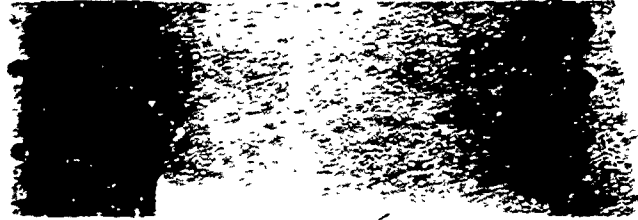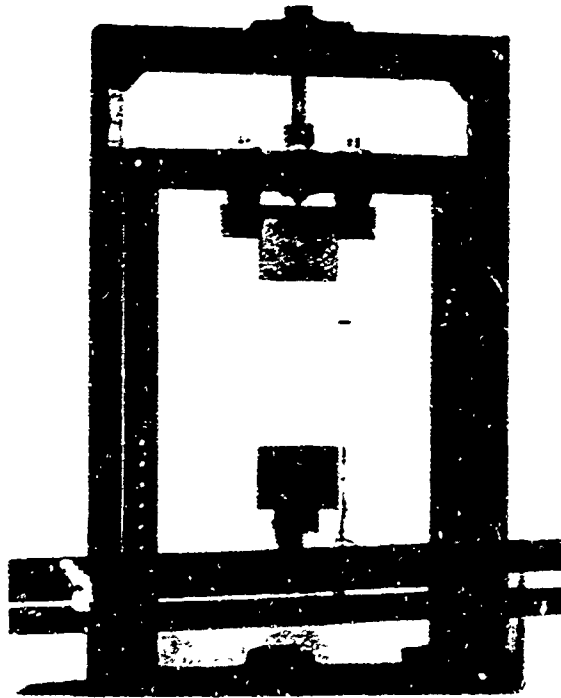
9

Figure 2. One model with loading plates.

Figure 3. One model in loading frame.

10

bearing load was then added to the side of the projection. As this load was increased, in many cases, the fringe order became too large to read and then the tension and bearing loads were reduced proportionally to produce the correct loading factor. For this test the tensile stress was calculated from the 4" wide section and bearing stress based on the full 3/4" projection height. A schedule of the applied stresses is shown in Table I. Both light and dark field photographs (some of which are shown in Figures 4, 5 and 6) were taken to allow the order to be read to the nearest 1/4 fringe. In some cases it became necessary to plot the fringe order as a function of distance and extrapolate to the edge to find the fringe order.

The fringe orders read off the photographs were normalized to the 200 pound tension load level and divided by the nominal tension fringe order at that load. The resulting stress concentration factors (K_T) are shown in Table II.

The $\overline{W}$ = 5 data represents a deviation from the above procedure. At the time the data was taken, it was felt that a method of superposition could be justifiably used, and this data was obtained by applying the two loads separately and adding the proper fringe orders to obtain the desired stress concentration factor. The K_T values shown in Figure 7 were obtained from one set of bearing load data and one set of tension load data and intermediate points faired between the $\overline{L}$ = 0 and $\overline{L}$ = 2 extremes. It was felt that this should be checked so, after all other data was taken, a sixth model was fabricated for $\overline{W}$ = 5 and $\overline{R}$ = 0.5. Only this result is shown on the final curves as specific points.

11

TABLE I

The actual stress values applied to the models during testing.

	$\overline{L} = 0$		$\overline{L} = .66$		$\overline{L} = 1.33$		$\overline{L} = 2.0$	
	σ^T	σ^B	σ^T	σ^B	σ^T	σ^B	σ^T	σ^B
$\overline{W} = 1/2$								
$\overline{R} = 1.0$	200	0	200	133	200	266	200	400
.8	200	0	200	133	200	266	200	400
.5	200	0	200	133	200	266	100	200
.3	200	0	200	133	100	133	50	100
.1	200	0	100	66	100	133	50	100
$\overline{W} = 1$								
$\overline{R} = 1.0$	200	0	200	133	200	266	200	400
.8	200	0	200	133	200	266	200	400
.5	200	0	200	133	200	266	200	400
.3	200	0	200	133	200	266	100	200
.1	200	0	200	133	100	133	100	200
$\overline{W} = 3$								
R = 1.0	200	0	200	133	200	266	200	400
.8	200	0	200	133	200	266	200	400
.5	200	0	200	133	200	266	200	400
.3	200	0	200	133	200	266	200	400
.1	200	0	200	133	100	133	100	200
$\overline{W} = 5$								
$\overline{R} = 1.0$	240	0						
.8	240	0						
.5	240	0						
.3	240	0						
.1	240	0						

This data calculated from bearing stress data without simultaneous tension stress by super-position.
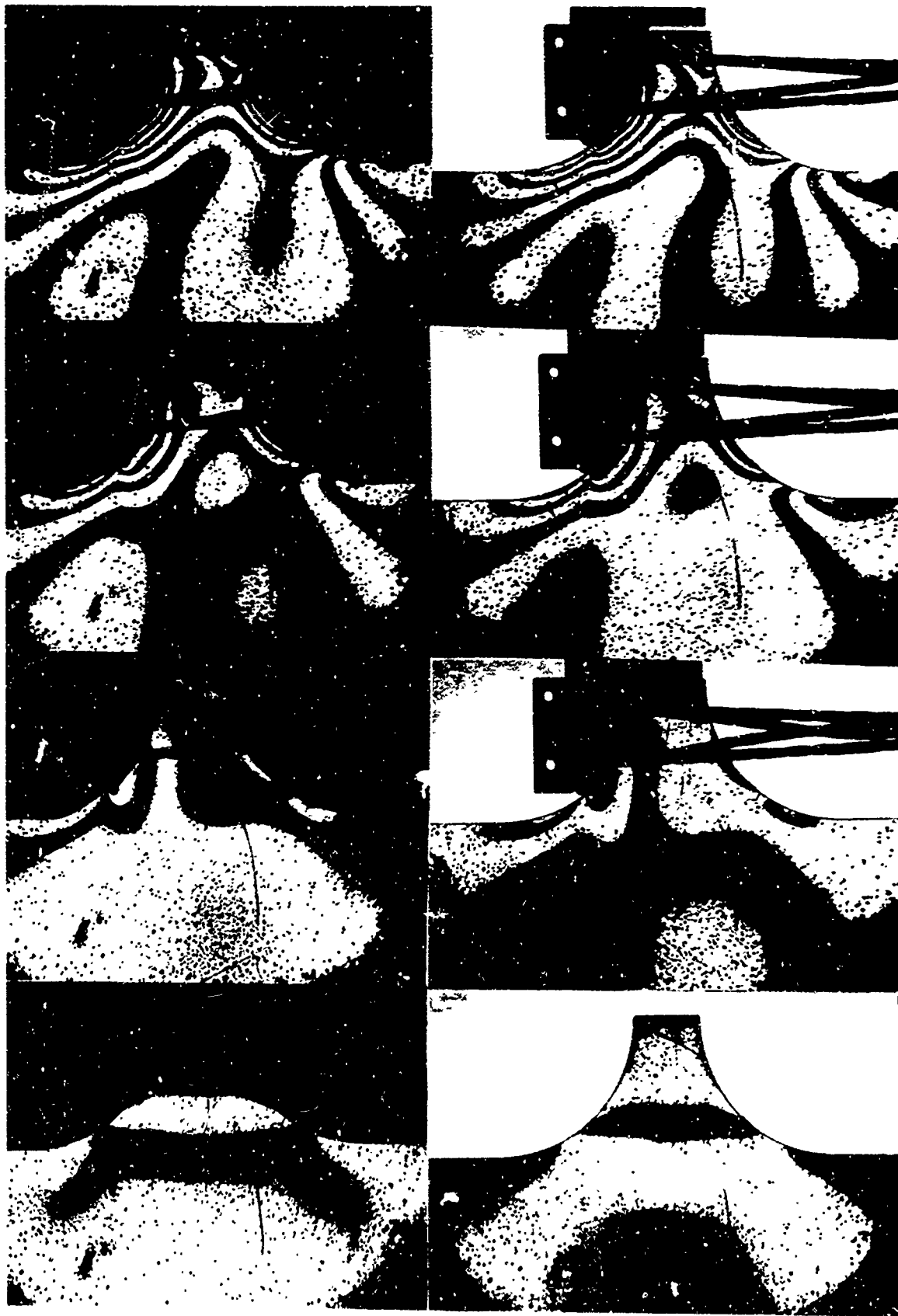
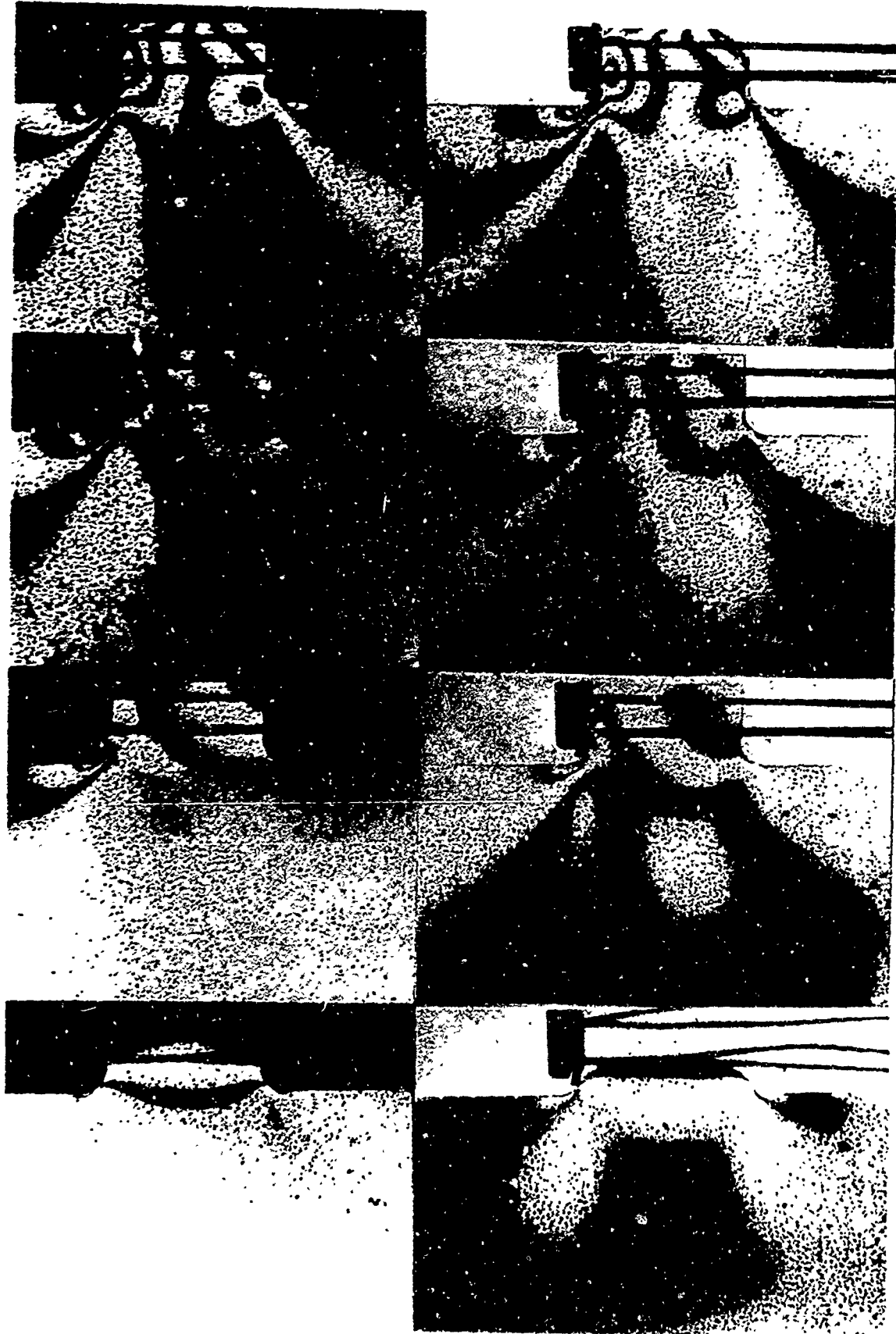Figure 4. Fringe photographs for the $\bar{W} = 0.5$, $\bar{R} = 1.0$ condition.

13
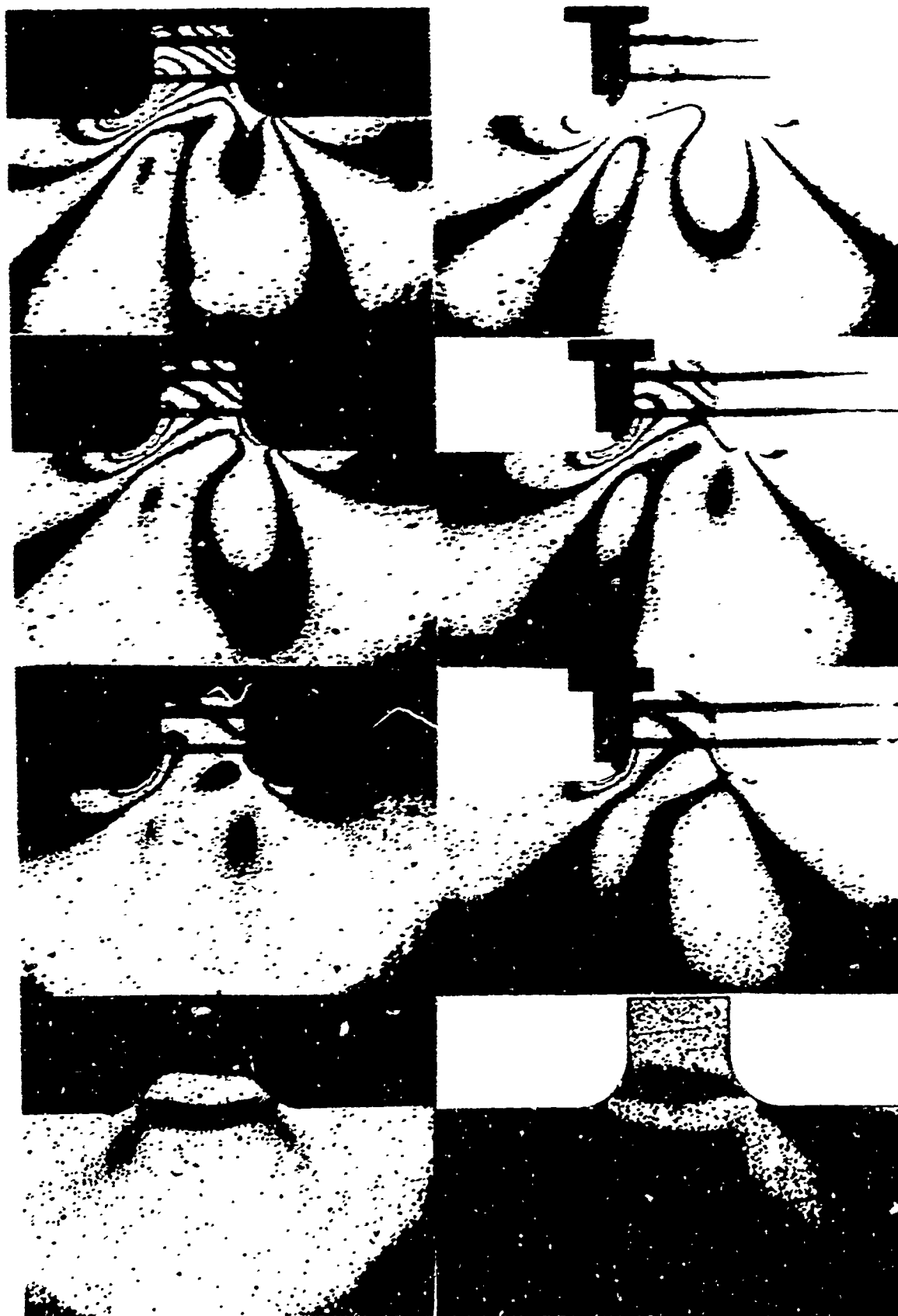
Figure 5. Fringe photographs for the $\bar{W} = 1.0$, $\bar{R} = 0.5$ condition.

$\bar{L} = 0$ 0.66   1.33   2.00

14

Figure 6. Fringe photographs of the $\overline{W} = 2.0$, $\overline{R} = 0.3$ condition

$\overline{L} = 0$ 0.66   1.33   2.00

TABLE II

Raw data as recorded from the fringe order readings.

	$\overline{L} = \underline{0}$	$\overline{L} = \underline{.66}$	$\overline{L} = \underline{1.33}$	$\overline{L} = \underline{2.0}$

$\overline{W} = 5$

$\overline{R}$

	$\overline{L} = \underline{0}$	$\overline{L} = \underline{.66}$	$\overline{L} = \underline{1.33}$	$\overline{L} = \underline{2.0}$
1.0	1.92	2.96	4.00	5.04
0.8	1.51	2.56	3.59	4.63
0.5	2.05	3.43	4.80	6.19
0.3	2.43	4.01	5.58	7.16
0.1	2.13	4.22	6.30	8.37
0.5 Model #6 (see text)	1.78	2.68	4.12	5.35

$\overline{W} = 2$

1.0	1.24	1.72	2.76	3.63
0.8	1.26	2.34	3.05	4.12
0.5	1.64	2.74	4.19	5.58
0.3	1.60	3.03	4.46	6.22
0.1	1.73	5.38	7.65	10.70

$\overline{W} = 1$

1.0	1.17	1.83	2.83	3.83
0.8	1.25	2.43	3.60	4.86
0.5	1.19	2.89	4.59	6.46
0.3	1.37	3.77	7.19	10.60
0.1	1.26	5.04	12.20	16.40

$\overline{W} = 1/2$

1.0	1.02	2.04	3.23	4.42
0.8	1.05	2.45	3.85	5.42
0.5	1.04	3.99	8.85	14.90
0.3	1.04	8.16	16.70	24.30
0.1	1.12	12.70	25.40	33.40

16

RESULTS

The data was plotted as a graph of stress concentration (K_T) versus loading factor ($\overline{L}$) for each value of radius, $\overline{R}$, and a line drawn in for each radius. These plots are shown in Figure 7.

The $\overline{W} = 5$ data presented a problem in that it was limited and the bearing load data was not in the correct form. This condition was further complicated by the large scatter in the data, particularly the tensile load ($\overline{L} = 0$) information. An attempt to use superposition to get stress concentration yields the results shown as raw data in Table II. The scatter is not unreasonable considering the low fringe order and the difficulty in applying the tensile load evenly across the sheet. It seemed desirable, in terms of the data for other values of $\overline{W}$, to "smooth" this data.

To accomplish this, plots of K_T versus $\overline{R}$ were used. It was discovered that the tensile load data plotted well on semi-log paper and the bearing load data well on log-log paper. This was supported by similar (but less variable) data taken from the $\overline{W} = 2$ model. When the plots were complete, it became apparent that a sufficiently accurate line could not be drawn by eye for the tensile load data, as it could be for the bearing load data, so a least square line was calculated. The two lines (one for bearing load and the other for tensile load) were then used as a basis for constructing the K_T versus $\overline{L}$ plots. It also seemed advisable to make a small correction for the slight difference between the positions of the two maximum stress locations. The tensile maximum was reread at the point of maximum

17

bearing stress. The new reading was then corrected for the error in
the fringe pattern by using the percent error between the maximum stress
point and the least square line. The result of superposition between
the bearing stress line and the corrected tensile stress information
is shown in Table III and the published plots.

After all this information was obtained, the data was cross-
plotted as stress concentration (K_T) versus projection width, $\overline{W}$, and
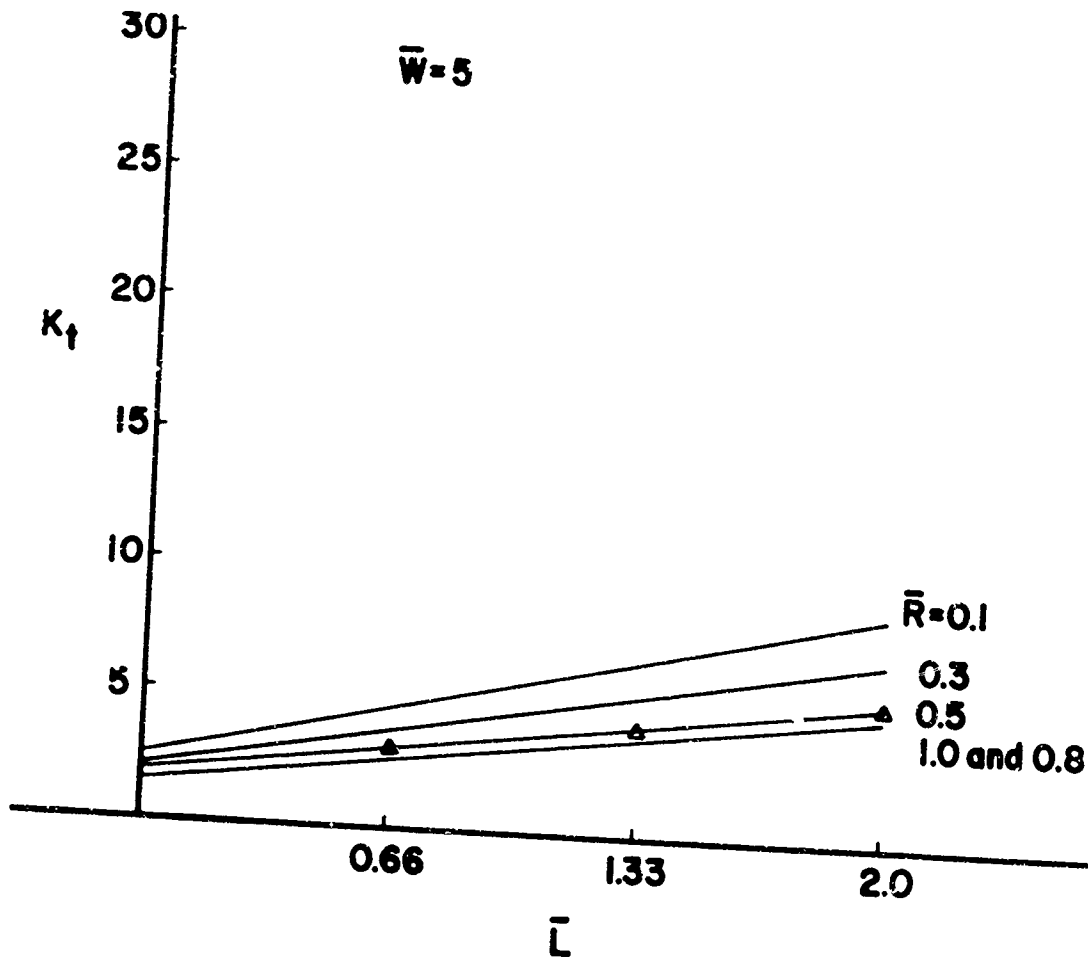these plots are shown in Figures 8 and 9.

Figure 7.   Basic plots of K_T vs. $\bar{L}$ for different levels of $\bar{R}$ at different levels of $\bar{W}$. (only the data points from model 6 are shown in the $\bar{W}$ = 5 plot.)
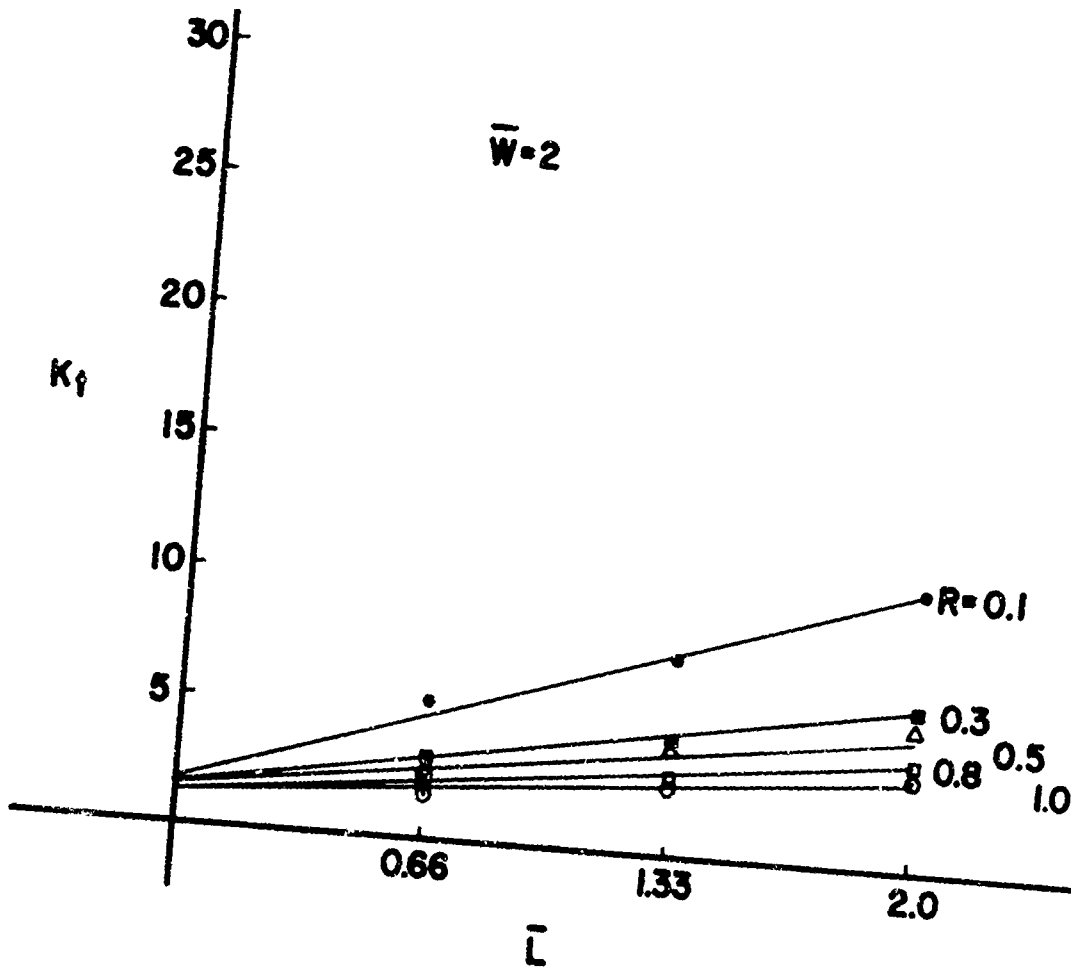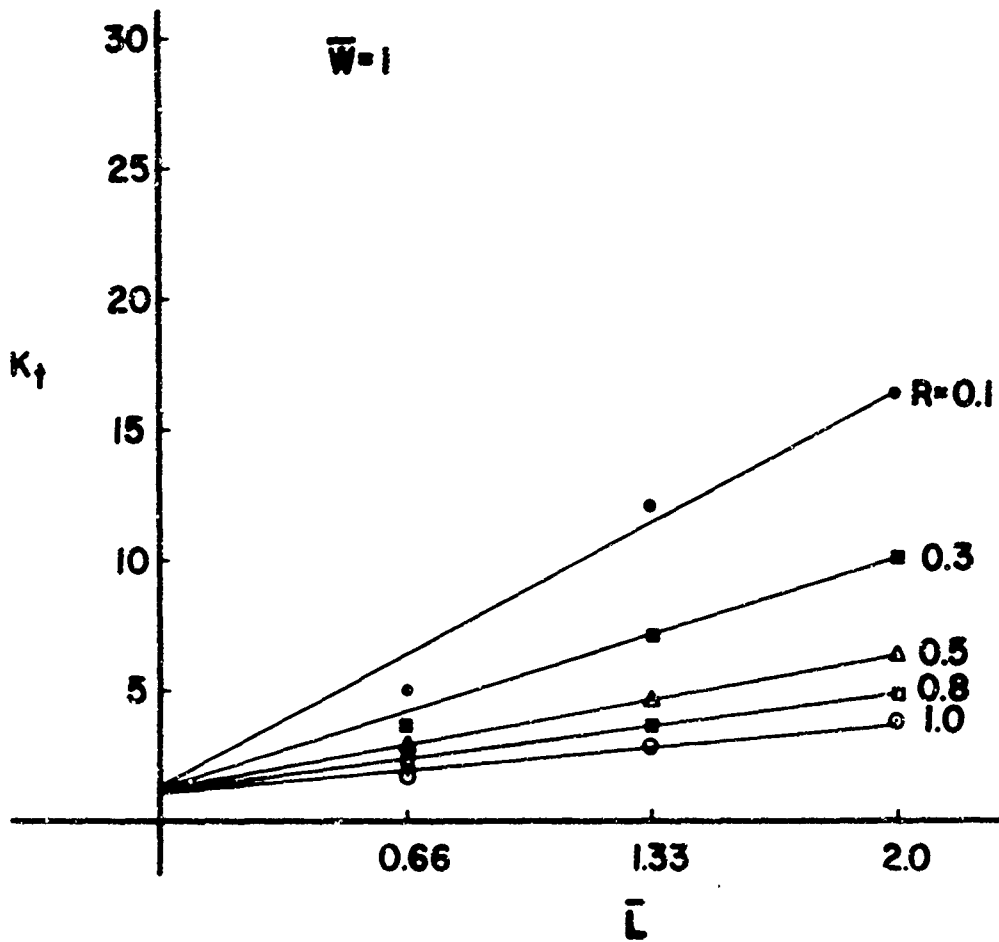
Figure 7. (continued) $\bar{W}$ = 2 plot.

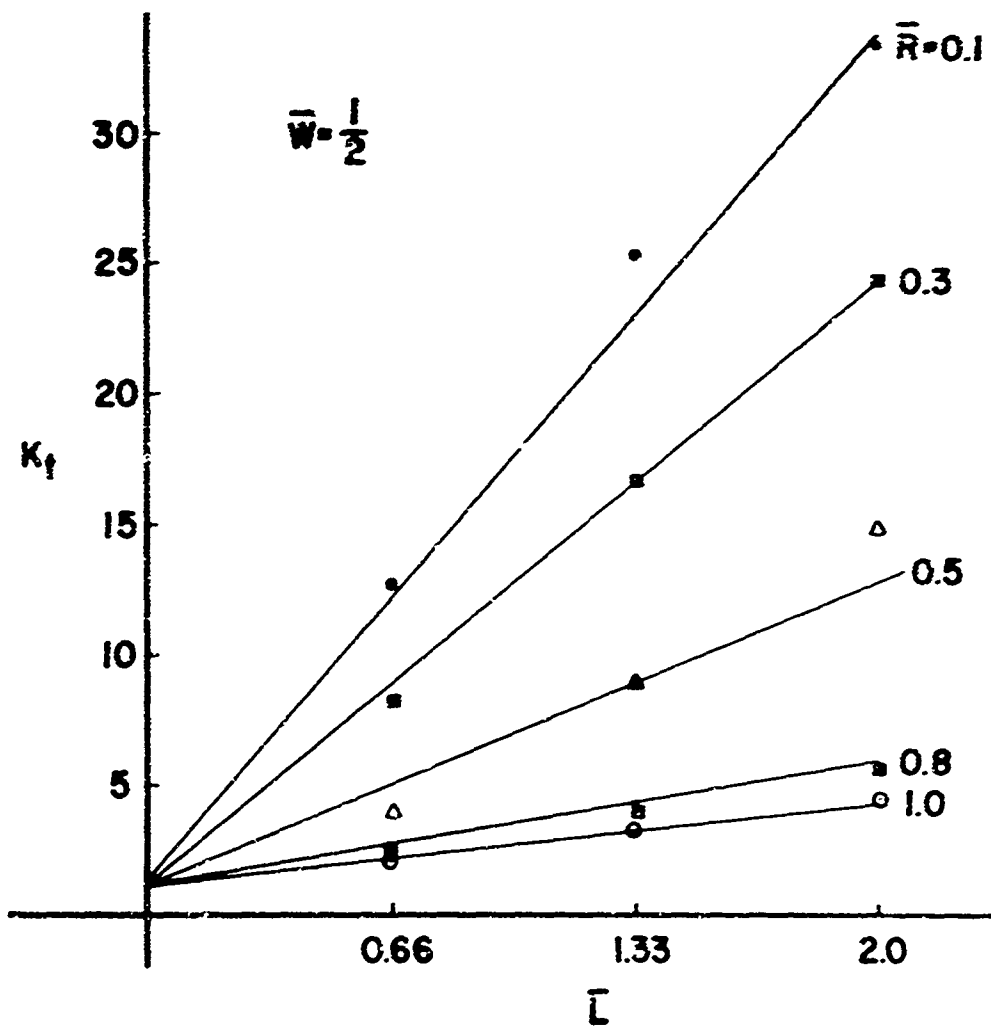Figure 7. (continued) $\overline{W} = 1$ plot.

21

Figure 7. (continued) $\bar{W} = \frac{1}{2}$ plot.

TABLE III

Data to be used to reproduce the published curves.

$\bar{R}$	$\bar{L} = 0$	$\bar{L} = .66$	$\bar{L} = 1.33$	$\bar{L} = 2.0$
$\bar{N} = 5$				
1.0	1.92	2.60	3.80	4.90
0.8	1.51	2.60	3.80	4.90
0.5	2.05	3.10	4.35	5.45
0.3	2.43	3.75	5.40	7.00
0.1	2.13	4.60	6.65	8.80
$\bar{N} = 2$				
1.0	1.24	2.00	2.75	3.50
0.8	1.26	2.20	3.25	4.10
0.5	1.64	2.70	3.40	5.00
0.3	1.60	3.10	4.70	6.25
0.1	1.73	4.75	7.70	10.70
$\bar{N} = 1$				
1.0	1.17	1.95	2.85	3.80
0.8	1.25	2.40	3.60	4.90
0.5	1.19	2.90	4.65	5.45
0.3	1.37	4.20	7.15	10.10
0.1	1.26	6.45	11.50	16.50
$\bar{N} = 1/2$				
1.0	1.02	2.10	3.20	4.30
0.8	1.05	2.70	4.40	6.00
0.5	1.04	5.00	8.90	12.80
0.3	1.04	8.90	16.60	24.30
0.1	1.12	12.20	23.00	33.90

These values were read off the final plots used for this report; however, they should be usable for engineering purposes.
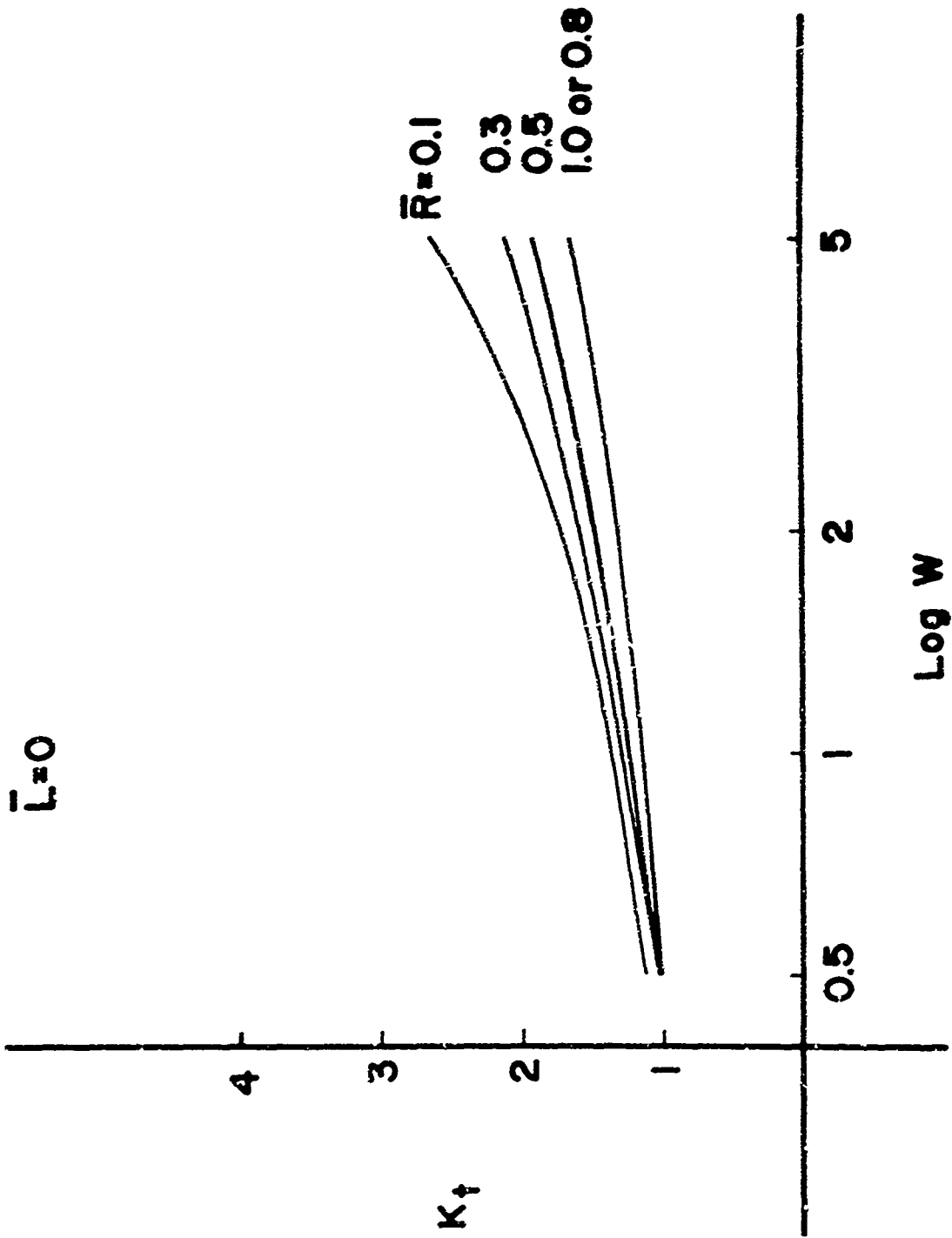
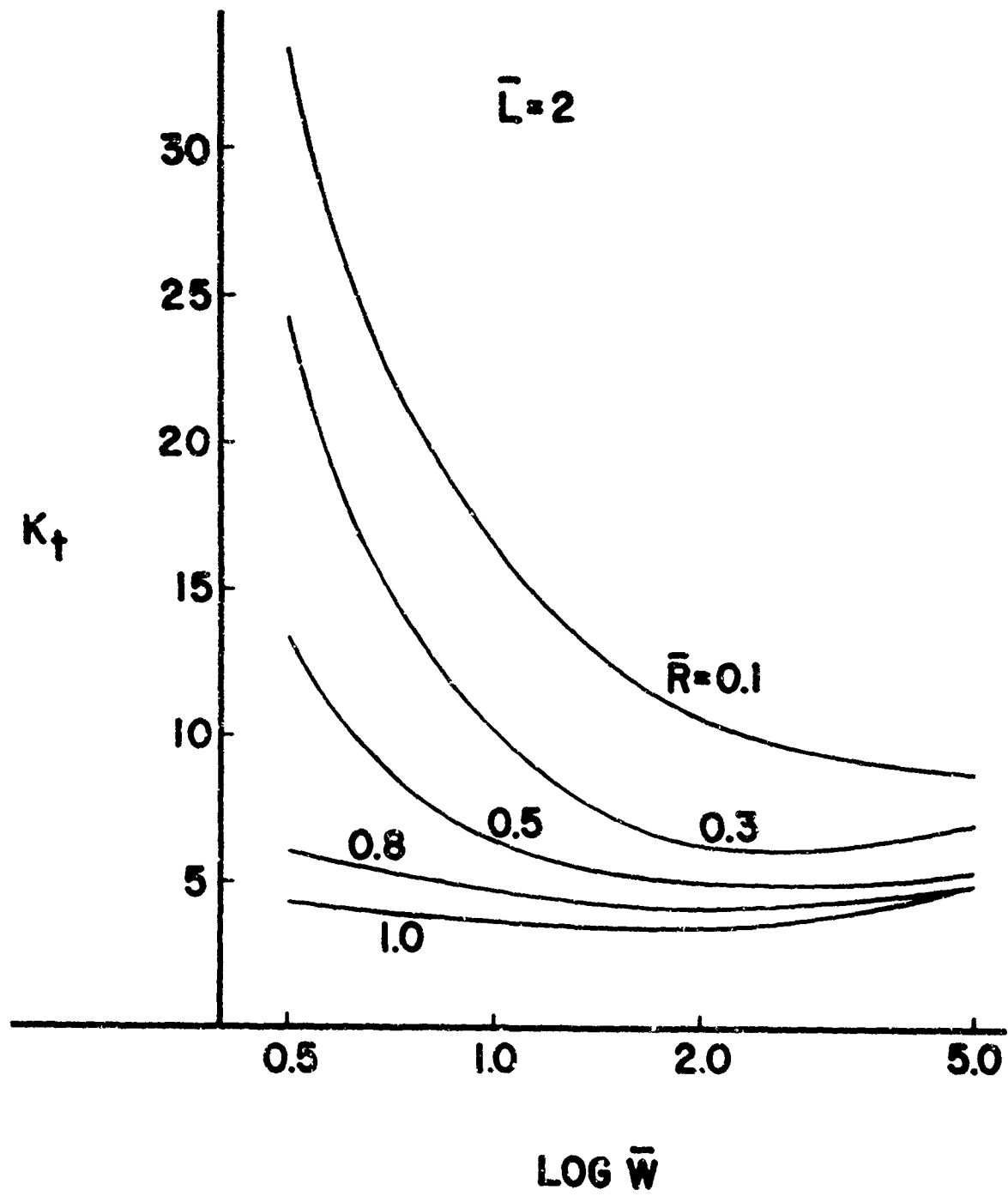Figure 8. Plot of K_T vs. $\bar{W}$ for different values of $\bar{R}$ at $\bar{L} = 0$.

Figure 9. Plot of K_T vs. $\bar{W}$ for different values of $\bar{R}$ at $\bar{L} = 2$.

DISCUSSION

It should be first noted that a very large range of geometry factors have been covered, and a large range of loading factors as well. This has been done with a rather small number of readings (30).

Looking at Figure 7, it may be seen that at large fillet radii (1.0 and 0.8) there seems to be very little improvement that can be obtained by increasing radius. However, at the small value (0.1 and 0.3), a large improvement can be accomplished with a modest change in radius. It can also be noted that the relative contribution of the tensile load stress concentration, as shown by the $\bar{L} = 0$ value, is of significant importance when the projection is very wide, but becomes less important as the projection becomes narrower. Looking at Figure 8, it can be seen that, when the loading factor is 0 (no bearing load), stress concentration becomes larger as the projection grows wider; while for $\bar{L} = \infty$ (no general tensile field), the general trend of stress concentration would obviously become smaller as the projection grows larger. However, when the two basic effects are added, as shown in the curve for $\bar{L} = 2$ (Figure 9), a slight minimum is obtained within the range of this experiment. The effect is not large because of the extreme domination of the bearing load on the overall stress concentration factor.

While the data in general looks good, the lines for different radius levels are not as evenly spaced as it would seem they should be. The author feels that this is due to slight unevenness of the loading across the face of the projection during some runs. This is supported

by the work of Heywood[3] where he shows a strong relation between fillet stress and the position of the loading on the projection.

In the process of evaluating the overall experiment, two things were done. First, was the fabrication of model 6 to check the $\bar{W}$ - 5 data. This data verified the information already obtained for this width. Second, the values were obtained for $\bar{L} = 0$, $\bar{W} = \infty$ from the work of Frocht as quoted by R. E. Pedersen[4]. This gives the value of K_T for only 4 of the radius levels. These values are:

R	K_T
1.0	1.83
0.8	1.97
0.5	2.30
0.3	2.76

These values are all higher than the values shown in Figure 8 for $\bar{W} = 5$, which shows a continuing increase in K_T before K_T levels off at the values for very wide projections.

The most interesting concept, perhaps, buried in the details of this investigation, is the ability to obtain the stress in any rifling at different points in the bore. After selecting a point in the tube and the rifling geometry, determine $\bar{W}$ and $\bar{R}$ and select the plot in Figure 7 which fits your case best; then the difficult problem of finding $\bar{L}$ is apparent. However, with the knowledge of the ballistic curve for the gun in question, and information available from references 1, 2 and 3, or other similar sources, it should be possible to establish the tangential stress (σ_T) and the bearing stress (σ_B); and a simple division process will then give $\bar{L}$. It should then be possible to find an estimate of K_T. This value of K_T multiplied by

27

tangential stress will give the maximum stress for that geometry. Table III gives values taken from the curves of Figure 8, and can be used by the design engineer to reproduce Figures 7, 8 and 9 in any appropriate scale.

In looking at Figures 4, 5 and 6, careful note should be taken of the position of the maximum stress point. It should be noted that at $\overline{L} = 0$, the maximum stress is very near the tangent point between the fillet and the main body of the model. However, as the bearing load is applied, the maximum stress moves closer to the center of the fillet. This indicates that the point of crack initiation may be different in a hydraulic fatigue test than an actual firing test, which includes the influence of bearing stress from the projectile.

The last point is the question of the effect of many projections in a series as is the case of rifling in a tube and not the single projection of the test. This is a rather complex problem but several things can be pointed out:

1. The stress concentration factor for a long series of notches is lower than that for a single notch.

2. In rifling, the space between two projections is usually greater than 1.5 times the width of the projection.

3. The stress concentration approaches the single notch value as the relative spacing becomes larger.

4. For any given width of tooth, the relative spacing becomes larger as the fillet radius becomes smaller.

28

From these and other considerations, some things seem apparent. First, for any given projection width the percent reduction in stress concentration will be larger for the larger radii values which are already low. Secondly, the effect becomes smaller in magnitude as the projection becomes wider. An examination of the data available on multiple discontinuities in reference(5)may help the design engineer to estimate the magnitude of the reduction in stress for his geometry.

CONCLUSIONS

The dual loading technique has successfully been used to define a large volume of the K_T, $\bar{L}$, $\bar{W}$ space for a large range of $\bar{R}$, with rather small number of tests. The chief error seems to be in the difficulty in loading the tooth accurately and this should be carefully checked in future testing.

The curves clearly show the relative merits of increasing the fillet radius. In all cases there is little to be gained by making the radius larger than 0.8 times the height of the projection, while the increase in stress, with the radius decreasing to less than 0.5 times the height, is very striking.

As the width is varied over the range of 0.5 to 5 times the height, and for radii larger than 0.1 times the height ($\bar{R}$ = .1), there is an optimum width near two times the height. However, the values of stress concentration do not vary a great deal in this region; this gives the designer a wide range of parameters which will produce similar stress concentration values.

ACKNOWLEDGMENT

The author wishes to thank Mr. T. Maclaughlin for his technical assistance and Mr. D. Kosinski for his work in the fabrication of the model.

REFERENCES

1. D. Radkowski, Bluhm and Bowier, "Thick-Walled Cylinder Handbook," Watertown Arsenal Laboratory, 1954.

2. Oerlikon Pocket Book, William Clowes and Sons, Limited, London, 1958, pp. 92-94.

3. Ballersen, C. E., "Principles of Firearms," John Wiley and Sons, Inc., New York, 1945, pp. 14 and 15.

4. Heywood, R. B., "Tensile Fillet Stress in Loaded Projections," Prod. Institute of Mechanical Engineering, 1949, Vol. 160, page 124.

5. R. E. Pedersen, "Stress Concentration Design Factors," John Wiley and Sons, Inc., New York, first edition 1962, page 66.

DOCUMENT CONTROL DATA - R & D

(Security classification of title, body of abstract and indexing annotation must be entered when the overall report is classified)

1 ORIGINATING ACTIVITY (Corporate author)	2a. REPORT SECURITY CLASSIFICATION
Watervliet Arsenal Watervliet, N.Y. 12189	Unclassified
	2b. GROUP

3 REPORT TITLE

TWO-DIMENSIONAL PHOTOELASTIC INVESTIGATION OF STRESSES IN RIFLING PROJECTIONS

4 DESCRIPTIVE NOTES (Type of report and inclusive dates)

Technical Report

5. AUTHOR(S) (First name, middle initial, last name)

G. Peter O'Hara

6 REPORT DATE	7a. TOTAL NO. OF PAGES	7b. NO OF REFS
April 1969	32	5

8a. CONTRACT OR GRANT NO.	9a. ORIGINATOR'S REPORT NUMBER(S)
AMCMS No. 5025.11.29900	
b. PROJECT NO.	WVT-6905
DA Project No. 1C024401A349	
c.	9b. OTHER REPORT NO(S) (Any other numbers that may be assigned this report)
d.	

10. DISTRIBUTION STATEMENT

This document has been approved for public release and sale; its distribution is unlimited.

11. SUPPLEMENTARY NOTES	12. SPONSORING MILITARY ACTIVITY
	U.S. Army Weapons Command

13 ABSTRACT

The problem of stress concentrations in rifling projections, caused by two independent simultaneous loads, is investigated experimentally using the two-dimensional photoelastic technique. A tensile field stress and a side bearing stress were applied to a series of photoelastic models and stress concentration determined for a large range of widths and fillet radii.

The stress concentration factor is presented in terms of non-dimensional width, non-dimensional fillet radius and a factor relating the two loads. This presentation clearly shows the decrease in stress concentration with increasing fillet radius and width, which allows the design engineer to evaluate the trade-offs of changing fillet radius or width in establishing the shape of rifling projections.